Metal localisation in gastropods shells: New insights from mass spectrometry techniques

Maëva Marimoutou, Juliette Oriot, Patrick Baldoni-Andrey, Gilles Bareille, Amiel Boullemant, Clémentine Gelber, Cecile Courreges, Sandra Mounicou, Hélène Tabouret, Séverine Le Faucheur

Metal localization in gastropods shells: new insights from mass spectrometry techniques

*Maëva Marimoutou[1], Juliette Oriot[1], Patrick Baldoni-Andrey[2], Gilles Bareille[1], Amiel Boullemant[3], Nick Gurieff[4], Clémentine Gelber[2], Cécile Courrèges[1], Sandra Mounicou[1], Hélène Tabouret[1], Séverine Le Faucheur[1]

[1] Universite de Pau et des Pays de l'Adour, E2S-UPPA, CNRS, IPREM, Pau, France

[2] TotalEnergies OneTech Pole d'Études et de Recherche de Lacq, France

[3]BCenv, Gardanne, France

[4] Rio Tinto Closure, France

KEYWORDS: Fs-LA-ICPMS, ToF-SIMS, *Radix balthica,* mollusk, shell layers, freshwaters

ABSTRACT

Gastropod shells are calcified structures made of several crystal layers. They grow throughout the lifecycle of mollusks by integrating some of the chemical elements present in their environment, including metals. This characteristic means mollusks can be useful bioindicators of metal exposure. The present study aimed to better understand the role of layer composition on metal accumulation. To that end, the gastropods *Radix balthica* were collected in a French river adjacent to a municipal wastewater treatment plant. Microchemical metal analyses in the different shell layers were performed by Femtosecond-Laser Ablation Inductively Coupled Plasma Mass Spectrometry (Fs-LA-ICP-MS) and analyses of the molecular environment of the metals were performed by Time-of-Flight secondary Ion Mass Spectrometry (TOF-SIMS). Strontium, Ba and Mn were well distributed within the whole shell and the high concentrations of these elements were found to be related to the aragonite structure of the shell. Copper, Ni, Pb and Zn were mostly present at the outer surfaces of the shell where the organic constituents were more concentrated. The analysis of metal distribution in shell layers could improve our understanding of the relationships between metal exposure and accumulation in mollusks, therefore providing evidences of their use as powerful integrated bioindicator of metal contamination.

SYNOPSIS

This study provides knowledge of metal accumulation in gastropod shells to improve their applicability as bioindicators of metal contamination in aquatic ecosystems.

INTRODUCTION

In freshwaters, gastropods are ubiquitous and represent the largest group of the phylum *Mollusca*, with over 4000 species being identified. As primary consumers, they have an important ecological role with the grazing on biofilms and detritus, and as sources of food for tertiary consumers such as fish [1]. In terms of water quality biomonitoring, mollusks possess several characteristics that make them particularly interesting as bioindicators: they are sessile, easy to collect and are sensitive to water quality modification [2, 3]. As such, many studies have focused on their use to evaluate metal exposure in freshwater and marine ecosystems [3, 4]. One particular biomonitoring approach involves the analysis of metals in soft tissues as a proxy of metal contamination of the ambient environment [5, 6].

Besides soft-tissues, another approach relies on the use of metal accumulation in the shell [7-9]. Shells are biomineral structures, which bring protection from physical and chemical aggression to mollusks. They grow throughout their life and are known to record changing environmental conditions [10-13]. For example, good correlations were observed between Cu, Zn, Co, Mn and Ni concentrations in the whole shell of freshwater bivalves (*Velesunio angasi)* and their respective concentrations in the water surrounding of a copper-uranium mine in Australia [14]. Nevertheless, the direct relationships between metal accumulation in the whole shell and the ambient media are not always straightforward [7, 12]. One of the possible explanations of this discrepancy might come from the different structures found in a shell. An average shell is composed at 95-99 % of minerals ($CaCO_3$) and at 0.1 – 5% of organic fraction (proteins, polysaccharides and chitin)[15, 16]. It is formed by several layers with different crystallization and composition from the outer to inner surface, *i.e.*, the periostracum (a protective organic layer), the prismatic layer (a mineral structure composed of aragonite or calcite depending on the species), and the nacreous layer (a

mineral structure composed of aragonite, which is directly in contact with the mantle and the soft body). Several microchemical studies focusing on growth layers of shell outer surfaces successfully demonstrated that Ba, Mg, Mn and Sr accumulation were potential proxies of environmental factors involved in the elemental marine biogeochemical cycle, such as temperature variation [17] or algal blooms [18-20]. In aragonite bivalve shell surfaces of the Manila clam *Ruditapes philippinarum*, the Ba/Ca ratio measured using Laser Ablation Inductively Coupled Plasma Mass Spectrometry (LA-ICPMS) has been demonstrated to be a proxy for the salinity variation in estuaries [12]. In that case, Mg/Ca and Sr/Ca ratios were not correlated to the ratios found in water and were then concluded to be under physiological control [12]. Another work reported an enrichment of Ba into the shell outer surface measured by Femtosecond Laser Ablation Inductively Coupled Plasma Mass Spectrometry (Fs-LA-ICPMS) of the great Scallop *Pecten maximus* as a function of the Ba concentration in water [21]. Trace metal accumulation was also examined with microanalysis techniques. In the bivalve *V. angasi*, the Cu, Mn, Zn concentrations in the surface of annual laminations were measured by dynamic secondary ion mass spectrometry (SIMS) and were found to be representative of the ambient environment at each studied year [14]. However, in that case, no correlations were observed for Pb and Fe. Very few studies have examined metal concentration as a function of shell layers, *i.e.* their distribution across the continuum periostracum, inner layers and inner surface in contact with the soft body. In *Mytilus edulis* shell, Pb concentration was found to decrease when the distance from the outer shell increased, highlighting the importance of taking into account metal distribution through the shell section to avoid concentration bias in microchemical analyses of shells [4].

The LA-ICPMS analytical technique allows the detection and quantification of surface elements with a high spatial resolution at the micrometer scale [22, 23]. One of the other advantages

of LA-ICPMS is the high-resolution multi-element mapping, which allows the analysis of metal distribution not only based on a transect measurements but on a larger surface [23]. Femtosecond-LA-ICPMS was successfully used for the study of biomineral composition, especially for bivalve shells [24-26], fish otoliths[27, 28] and corals[29, 30]. Time of Flight (ToF)-SIMS is an extreme surface and depth semi-quantitative analysis (nanometer scale) of elements and molecules in solid samples [31]. In biological samples, its main advantage relies on the detection of molecules such as protein and peptide fragments, which might provide information on the composition of the shell's organic matrix [32]. To the best of our knowledge, this analytical approach has never been used for biomineral studies. The aim of this work was (1) to examine metal distribution in the different shell layers using Fs-LA-ICPMS, and (2) to identify the molecular environment of these metals using ToF-SIMS in order to better understand the processes of metal accumulation in shells. The gastropod *Radix balthica* (Linnaeus, 1758) was the organism of interest as it is a ubiquitous species of Europe rivers. Native organisms were collected in the mixing zone of a wastewater treatment plant (WWTP) and the Gave de Pau river and then examined for shell metal distribution using Fs-LA-ICPMS and ToF-SIMS.

MATERIAL AND METHODS

Study area and collected organisms

The field experiment was conducted in May 2021 in the Gave de Pau river (France) at the discharge point of a wastewater treatment plant (WWTP). On the day of the gastropod sampling, the Gave de Pau river had a pH of 7.21 ± 0.09, the conductivity was at 430 $\mu S \cdot cm^{-1}$, the temperature was at 17.2 °C and the DOC concentration was 13 ± 2 $mg \cdot L^{-1}$. Measurements of Ca and Mg concentrations were 45.8 ± 0.1 and 4.29 ± 0.01 $mg \cdot L^{-1}$, respectively. Measured dissolved

metal concentrations were 16 ± 2 $\mu g \cdot L^{-1}$ Ba, 0.9 ± 0.1 $\mu g \cdot L^{-1}$ Cu, 0.71 ± 0.02 $\mu g \cdot L^{-1}$ Co, 0.010 ± 0.004 $\mu g \cdot L^{-1}$ Cd, 5.16 ± 0.06 $\mu g \cdot L^{-1}$ Li, 288 ± 46 $\mu g \cdot L^{-1}$ Mn, 1.94 ± 0.33 $\mu g \cdot L^{-1}$ Ni, 1.62 ± 0.05 $\mu g \cdot L^{-1}$ Pb, 182 ± 2 $\mu g \cdot L^{-1}$ Sr and 40 ± 3 $\mu g \cdot L^{-1}$ Zn.

A total of 12 native *Radix balthica* adults (length: 11.2 ± 0.6 mm; width: 7.7 ± 0.7 mm) were collected by hand within an area of about 1 m^2 taking care to select individuals of a similar size and brought back to the laboratory in river water and at ambient temperature. They were then depurated for 3 days in river water collected upstream of the WWTP and were stored at -20°C without further preparation until analysis.

Determination of shell structure by Scanning Electron Microscopy (SEM)

For SEM analyses, the shell was fractured at the peristome region, which corresponds to the most recent part of shell, and was sputtered with gold. The shell layers were identified by observation of the difference between the types of microstructures. Additionally, one of the shell sections embedded in resin for Fs-LA-ICPMS (see section *Shell Fs-LA-ICPM analysis*) was also analysed. To that end, samples were sanded for 10 minutes at 10 kV using a SC-2000 ion polisher (Technoorg Linda, Budapest, Hungary) and were observed with a Apréo 2 scanning election microscope at 500 V (Thermofisher, Waltham (MA), USA).

Metal spatial distribution and concentrations in shells using Fs-LA-ICPMS analysis

Shells (n=3) were separated from soft tissues using two tweezers and were rinsed with ultrapure water. They were then washed for 12 hours in 1 mL of 2 % hydrogen peroxide (H_2O_2) (Ultratrace analysis 30 %, Merck). This washing procedure was selected after an optimization step based on the rinsing agents (acetic acid and H_2O_2) and contact time (Figure S1). After

drying under a laminar flow hood, the whole shells were embedded in an epoxy resin (Araldite 2020, Huntsmann). Once dried, the embedded shells were sanded with abrasive papers of decreasing grain sizes (120, 800, 1200, 2400, and 4000 grit, Escil) until a fine cross-section was obtained from the apex to the aperture. Cross-sections were rigorously rinsed with ultra-pure water, dried and stored at room temperature. Laser ablation analyses were performed using an IR 1030 nm Fs-LA (Alfamet-Novalase, Bordeaux, France) coupled to an ICPMS (Agilent 8900 ICP-MS Triple Quad, Les Ulis, France). The laser was set at a pulse frequency of 50 Hz with an ablation width of 20 µm and a speed of 60 $\mu m \cdot s^{-1}$. Eleven isotopes were monitored: ^{7}Li, ^{43}Ca, ^{55}Mn, ^{58}Ni, ^{59}Co, ^{63}Cu, ^{66}Zn, ^{86}Sr, ^{111}Cd, ^{138}Ba and ^{208}Pb. External calibrations were performed using NIST614, NIST612 and NIST610 certified synthetic reference glasses (National Institute of Standards and Technology, Gaithersburg (MD), USA). Analytical accuracy was verified using calcified reference materials, which were fish otoliths FEBS-1 (National Research Council of Canada, Ottawa, Canada) and NIES22 (National Institute for Environmental Studies, Tsukuba, Japan) in absence of other relevant certified reference materials. The isotope ^{43}Ca was used as an internal standard to quantify variations in ablation performance. The measured recoveries were 93 ± 2 % and 91 ± 9 % for ^{86}Sr and ^{138}Ba, respectively. The detection limits of Li, Mn, Ni, Co, Cu, Zn, Sr, Cd, Ba and Pb were respectively 0.40, 0.18, 0.27, 0.40, 0.22, 0.98, 0.11, 0.30, 0.01 and 0.07 $\mu g \cdot g^{-1}$. A time resolved analysis mass spectrum was acquired for each transect and was extracted under csv format files. Several 20 µm-wide transects were made parallel to the shell section in the most recent part of the shell in order to cover the entire area of the section required to generate the elemental image (Figure S2). Elemental maps were made using an Excel VBA Macro (*Focal*; internal Macro developed by Dr C. Pécheyran, IPREM, Pau, France) enabling the processing of the csv files. The obtained maps were exported as text and were processed on

ImageJ (ImageJ, 1.51, National Institutes of Health, Bethesda (MD), USA) to represent a color code map as a function of the concentration ($\mu g \cdot g^{-1}$) for each element present in the shells. The averages of metal concentrations were evaluated for each zone (outer surface, inner shell and inner surface) from the shell cross-sections. The method consisted of measuring the average concentration of 10 predefined shell areas (60 µm x 20 µm) for each zone (outer surface, inner shell and inner surface) by ImageJ.

Shell molecular and elemental analyses using ToF-SIMS

Shells were separated from soft tissues following the same procedure as for LA-ICPMS analysis. Two flat pieces of each replicate (approximatively 0.5 x 0.5 mm) of the last growth stria close to the peristome were cut using a wire cutter. One preparation was used to analyze the outer part of the shell and the other one was used to analyze the inner part. Both of them were directly fixed on the ToF-SIMS sample holder using double-sided tape. Analyses were performed using a TRIFT V NanoToF ©I (Physical Electronics, Chanhassen (MN), USA) equipped with a 30 kV Bismuth Bi_n^{q+} LMIG primary ion gun. Mass spectra were firstly acquired on three random zones of the outer and inner shell in both polarities for one individual in order to evaluate the homogeneity of the surface for one analysed portion of the shell. Then, mass spectra of the outer and inner shell in both polarities were recorded for all organisms (n=3) to evaluate the reproducibility between the 3 individuals. All mass spectra were acquired at room temperature in both polarities using Bi_3^{++} primary ions, 50 x 50 μm^2 field-of-view and 30 frames (dose: 2.2 x 10^{12} ions$\cdot cm^{-2}$) to perform semi-quantitative analysis (comparing the ratio of peaks intensities). Depth profile experiments (series of 40 "analysis/sputtering" cycles) were performed in positive polarity using the same previous analysis conditions and a 5 kV Ar^+ gas gun for

etching (with a sputtering time of 60 seconds for each cycle, over a 300 x 300 μm^2 area and a DC current of 500 nA). For all analyses, charge compensation (with low dose of e- and Ar^+) was applied to limit charging effects. ToF-SIMS data were processed using ToF-DR software (supplied by Physical Electronics). Positive polarity mass spectra were calibrated using $C_2H_2^+$ (m/z 26.02), $C_2H_3^+$ (m/z 27.02) and $C_3H_7^+$ (m/z 43.04) peaks. Negative polarity mass spectra were calibrated using OH^- (m/z 17.00), C_2H^- (m/z 25.00) and Cl^- (m/z 35.00) peaks. For the graphical representation of depth-profiles, the intensity of the secondary ions of interest was normalised related to the total ion counts. To better visualise the spatial in-depth distribution of the considered species, 3D images were reconstructed from depth-profile experiments. The signal intensity of elements and molecular secondary ions were plotted over the analysed area (50 µm x 50 µm = x and y dimensions) versus the etching time (the z axis, 1600 s, which is over dimensioned compared to the other axes). When the signal intensity of the secondary ion is lower than 1000 in the mass spectrum, the 3D reconstruction was not completed.

Statistical analyses

Statistical analyses were performed using Rstudio (Version 2022.07.2-554). The test ANOVA with and lsmeans post-hoc was carried out with the significance below 0.05 to compare metal concentration in the outer surface, inner part and inner surface between each organism (n=3) and the average values obtained taking into account all three organisms. Data normality was tested using the Shapiro-Wilk test and the homogeneity of variances using Bartlett's test.

RESULTS

Determination of shell structure

The different shell layers were visually identified using the difference of the crystal structures (Figure 1). The outer surface crystal (OS) structure was not clearly defined, which was indicative of a protein-rich layer. That layer was estimated to be ~ 3 µm thick. The inner part (IP), with a thickness of ~ 150 µm, was characterised by a crossed lamellar structure corresponding to a complex prismatic layer. The inner surface (IS) had a tablet structure of crystals of ~ 10 µm thick, characteristics of a nacreous layer [33-35]. Both crystal structures were thus characteristics of aragonite [15, 16, 36]. Note that the thickness of each layer could not be precisely determined because of the curveted surface of the studied shell section.

Metal spatial distribution and concentrations in shells

The elemental distribution measured by Fs-LA-ICPMS highlighted that metals were distributed differently within the gastropod shells (Figure 2). Strontium concentration was mostly homogeneous and no significant differences were measured between the outer (average concentrations of 3 individuals; Ravg = 235 ± 73 $\mu g \cdot g^{-1}$), the inner surfaces (Ravg = 317 ± 134 $\mu g \cdot g^{-1}$) and the inner part (Ravg = 298 ± 185 $\mu g \cdot g^{-1}$) ($p>0.05$) (Figure 3). Its concentration was significantly different between individuals ($p<0.05$). The highest concentration was measured in the replicate 2 – R2 (439 ± 133 $\mu g \cdot g^{-1}$). Among the studied elements, Sr was the most concentrated metal analysed. Barium and Mn were also detected at high concentrations with an average concentration of 23 ± 8 and 23 ± 18 $\mu g \cdot g^{-1}$ in the outer surfaces and 25 ± 11 and 20 ± 12 $\mu g \cdot g^{-1}$ in the inner surfaces, respectively (Figure 3). No significant differences were measured between those surfaces ($p>0.05$) (Figure 3). The concentrations in the inner part (Ba-Ravg = 9 ± 6 $\mu g \cdot g^{-1}$; Mn-Ravg = 7 ± 3 $\mu g \cdot g^{-1}$) were significantly lower than those found in the two surfaces. For both of them, the concentrations were significantly different between the organisms

($p<0.05$). Barium concentrations were higher in R2 (26 ± 17 $\mu g \cdot g^{-1}$) than in R3 and in R1 for all surfaces. Manganese presented similar distribution between organisms, except for the outer surface for which higher concentration was measured in R3 (47 ± 6 $\mu g \cdot g^{-1}$) than in R2 and in R1. The distribution of Zn and Cu were significantly different between the outer surfaces [Ravg(Zn)=23 ± 10 and Ravg(Cu)= 2.2 ± 0.8 $\mu g \cdot g^{-1}$], the inner surfaces [Ravg(Zn)=15 ± 10 and Ravg(Cu)=1.3 ± 1.1 $\mu g \cdot g^{-1}$] and the inner part (Ravg(Zn) = 1.7 ± 0.6 $\mu g \cdot g^{-1}$ and Ravg(Cu) = 0.13 ± 0.11 $\mu g \cdot g^{-1}$] ($p<0.05$). For both elements, the R1 and R2 had similar concentrations ($p>0.05$). The highest concentrations of Pb (Ravg =2.7 ± 0.9 $\mu g \cdot g^{-1}$) and Ni (Ravg =3.5 ± 1.5 $\mu g \cdot g^{-1}$) were mainly found in the outer surface compared to the inner part and the inner surface. Similar concentrations for Pb and Ni were observed between all individuals for each surface ($p>0.05$). Among all studied trace elements, Zn was measured at the highest concentrations compared to Cu, Pb and Ni. Lithium, Co and Cd were below the detection limits.

Shell molecular analyses

Further chemical analyses of shell surfaces were performed at the nanoscale (1-2 nm) level using ToF-SIMS. Firstly, the chemical composition of the outer and inner surfaces of one gastropod shell was characterised in both positive and negative polarities at three different random positions on the last growth stria, so that to check the homogeneity of the sample (Figure S3). The same analysis were reproduced for three gastropods to check the reproducibility between individuals (Figures S4). Similar chemical compositions were identified between the three random positions for one individual and for the three replicates of individuals. The same pattern was observed for both outer and inner surfaces in both polarities. Molecular shell composition was thus mostly homogenous for the portion analysed as well as between individuals. Therefore,

only results obtained for the replicate 1 surfaces in both polarities are presented in Figure 4. For the outer surface in positive polarity, peaks attributed to $C_2H_3^+$ (*m/z* 27.02), $C_2H_6^+$(*m/z* 29.04), Ca^+ (*m/z* 39.96), $C_3H_7^+$ (*m/z* 43.04) and $C_5H_{10}^+$ (*m/z* 70.04) were identified, which are characteristic of organic compounds (except for the calcium matrix). For the inner surface, the most intense peaks were Ca^+ and $CaOH^+$. In the negative polarity, the presence of phospholipid fragments PO_2^- (m/z 62.98) and PO_3^- (m/z 78.98) was observed for both surfaces (Figure 4). Moreover, the fragment CN^-, characteristic of peptide bond, was also detected on both surfaces. At higher *m/z* (130-420), more peaks were detected in both polarities on the inner surface than on the outer surface (Figures S5 and S6). These molecular fragments might be characteristic of fatty acid chains coming from the lipids and/or proteins of the soft body, which was in contact with the inner shell surface; further investigations using Tandem MS are currently under process to confirm the attribution of these higher m/z peaks.

To characterize the in-depth spatial distribution of the species of interest, etching experiments of the outer and inner surfaces of the shell were performed in the positive polarity (Figure 5). On the outer surface, Ca^+ was the dominant element detected throughout the etching. Organic fragment ($C_2H_3^+$) was only detected at the beginning of the etching, which implies it was only located at the extreme outer surface of the shell (Figure 5). Ba^+ was also detected with the highest intensity at the beginning at the etching, which shows it was mainly located at the extreme surface of the shell like organic matter; its 3D spatial distribution shows some heterogeneities but its concentration globally decreases with the etching. In the inner surface, Ca^+ was detected with a stable signal throughout the etching. Note that so far the detection and identification of other metals was not possible over the analysed areas and volumes of the shells;

matrix effects as well as charging effects due to the roughness of the sample make the analysis more complicated.

Tentative measurements of the etching depth were carried out using a profilometer (Still Confocal Chromatic Sensor, Aix-en-Provence, France) but could not be completed due to the roughness of the sample.

DISCUSSION

The Fs-LA-ICPMS analyses highlighted that metal distribution was mainly heterogeneous in the studied gastropod shells, except for Sr. This element is well-known for substituting Ca during shell formation due to its similar ionic radius (113 and 99 pm for Sr and Ca, respectively) [37,16]. Mollusks accumulate Sr in the mantle through food and water ingestion as well as through dermal contact [4]. Shell formation takes place in the extrapallial space, in which Sr is transported from the mantle using pumps (Ca^{2+}-ATPase). Strontium could then replace Ca to react with HCO_3^- and as such, participates into the shell formation [16]. Nevertheless, Sr accumulation in shells depends also on the shell carbonate polymorph. For example, in the pearl oyster *Pinctada radiata,* higher concentrations of Sr and Ba were measured in aragonite than in calcite [38]. That better increased affinity for aragonite was explained by the high ionic radius of Sr and Ba, which favors incorporation of these elements into the crystal structure [15, 35, 38]. The shell of the gastropods used in this study is mainly composed of aragonite as observed with SEM, which could partly explain the high Sr and Ba concentrations. Manganese was also measured in high concentrations in our studied shells in agreement with the literature [39, 40]. For example, higher shell Mn concentrations than Cu, Pb and Zn concentrations were also observed in the mussel *Perna perna* exposed to a series of seven metals [41]. Manganese is a common metal found in

shells and as a divalent cation, could also replace Ca to fit into the carbonate lattice structure [39, 40]. Nevertheless, shell Sr, Ba and Mn accumulation depends on several abiotic and biotic factors, such as their concentrations in the ambient environment and the organism shell growth rate, age and feeding rate [4, 16]. In the present study, dissolved Sr, Ba and Mn concentrations in the ambient water were much higher (> 150 $\mu g \cdot L^{-1}$) than those of the other studied metals, partly explaining the higher accumulation of these metals. In *Corbicula fluminea* shells, Sr accumulation was found to be controlled by temperature and the ambient Sr/Ca_{water} level whereas Ba accumulation was observed to be mediated by several variables such as temperature, food level, Ba/Ca_{water} level and the shell growth rate [17]. Some of these factors may play a role in the significant inter-individual variability observed for these elements in our study.

In contrast to Sr, Ba and Mn, trace metals (Cu, Ni, Pb and Zn) were mostly measured at the shell surfaces. Zinc and Cu were detected at high concentrations in the outer and inner shell surfaces whereas Ni and Pb were mainly measured in the outer shell surface. These results are in agreement with those obtained on bivalves for which, Pb and Cu were also found in high concentrations in the outer shell surfaces [4]. In the present study, molecular analyses of the shell surfaces performed with ToF-SIMS demonstrated the presence of organic constituents on both outer and inner surfaces, which was mostly composed of phospholipid and peptide fragments. This thin outer layer most likely corresponds to the periostracum, as observed with SEM, which is known to be mainly composed of conchiolin and chitin[16]. Trace metals have already been reported to be found in that organic fraction of the shell [4, 42]. Sturesson[43] studied Pb enrichment in *Mytilus edulis* shell as a function of the shell layers and showed that the highest Pb concentrations were observed in the periostracum formed during the exposure time. Sturesson thus suggested that Pb enrichment in shells took place through metal accumulation via the

mantle, and is governed by metabolic processes. The presence of biofilms growing onto the surface shell can also contribute to metal accumulation in the outer surface. Indeed, biofilms are also known to accumulate metals as a function of metal concentration in the ambient media. Nevertheless, that interference from specific biofilm metal sorption should be limited in this study through the application of the H_2O_2 washing step [44] as confirmed with the SEM analyses. Non-specific metal adsorption onto the shell surface could also occur due to the negative functional groups ($-COO^-$ and $-PO_4^{2-}$) detected with ToF-SIMS at the periostracum surface [43, 45] but cannot be distinguished from the specific adsorption. In both inner surfaces and parts, negligible concentrations of trace metals were measured, in agreement with the literature[4, 16].

Beside shell composition, trace metal distribution can also be modulated by the nature of the element itself, for example the affinity Cu and Pb have with carbonate. Similarly for Sr, Ba and Mn, shell formation rate and the quality of the ambient environment (element concentration, temperature, food availability) could also play a role in the incorporation [4, 17]. The physiological involvement of metals in mollusk development is another parameter that might also influence metal concentration in the shell [46]. Metals such as Cu and Zn are essential for gastropods and are thus metabolically highly regulated in bivalves [47]. Similar concentrations of Ni, Cu and Pb in the marine mussel *Bathymodiolus platifrons* shell also suggest a tight bioregulation of those elements in the soft body [37]. In organisms studied in this article, the metal concentrations in the shell were significantly different for Sr, Ba, Zn, Cu and Mn between organisms. However, trace element concentrations did not show such high variations between the organisms, which support the concept of the tightly controlled regulation during bioaccumulation [9].

The present study demonstrates the usefulness of coupling Fs-LA-ICPMS imaging analysis with ToF-SIMS analysis to better understand metal distribution in mollusk shells. A metal mapping

covering several shell layers were obtained with Fs-LA-ICPMS at the micro-meter scale, whereas the molecular environment of the metals was elucidated with the ToF-SIMS at the nano-scale level. That complementary use of techniques highlights the importance of organic constituents in metal accumulation in gastropod shells. Those results will allow us to implement a strategy for the analysis of shells on a larger scale. By focusing only on the analysis of metals on the outer surfaces of the shells, the cost and time of the analysis will be reduced while providing relevant information on exposure. Follow-up experiments will examine the relationships between metal concentrations in the ambient water and metal accumulation in shell in WWTP upstream, mixing zone and downstream to further evaluate the use of shell *Radix balthica* as a biomonitoring tool of metal contamination in freshwater.

AUTHOR INFORMATION

Corresponding Authors

* Maëva Marimoutou - Université de Pau et des Pays de l'Adour, IPREM, Pau, France

Email : maeva.marimoutou@univ-pau.fr

*Séverine Le Faucheur - Université de Pau et des Pays de l'Adour, IPREM, France

Email : severine.le-faucheur@univ-pau.fr

Author Contributions

Maëva Marimoutou: methodology, software, formal analysis, investigation, data curation, writing – original draft, visualization.

Juliette Oriot: methodology.

Gilles Bareille: conceptualization, writing – review & editing, supervision.

Amiel Boullemant: writing – review & editing.

Nick Gurieff: writing – review & editing.

Clémentine Gelber: review & editing.

Patrick Baldoni-Andrey: funding acquisition.

Cécile Courrèges: methodology, writing – review & editing.

Sandra Mounicou: writing – review & editing.

Hélène Tabouret: methodology, writing – review & editing.

Séverine Le Faucheur: conceptualization, methodology, writing – review & editing, supervision, project administration, funding acquisition.

Acknowledgment

The authors are very grateful to Patrick Baldoni-Andrey (TotalEnergies) and Nick Gurieff (Rio Tinto) for helpful scientific discussions. They also would like to thank Stellia Sebihi for providing help with the field sampling and sample preparation, Mathieu Milhe-Poutingon for the chemical analyses and Virginie Pellerin for the SEM analyses. We are grateful for Jean-Marc Dalens for his help with the species manipulation. This research was funded by the Research Partnership Chair E2S-UPPA-TotalEnergies-Rio Tinto (ANR-16-IDEX-0002).

ABBREVIATIONS

Cps, Count per second; (Fs)-LA-ICPMS, Femtosecond-LA-ICPMS; IP, the inner part; IS, inner surface; LA-ICPMS, Laser Ablation Inductively Coupled Plasma Mass Spectrometry; OS, outer surface; SEM, Scanning Electron Microscopy; ToF-SIMS, Time-of-Flight Secondary Ion Mass Spectrometry; WWTP, Wastewater Treatment Plant

REFERENCES

1. Pyron, M.; Brown, K. M., Introduction to Mollusca and the Class Gastropoda. In *Ecology and general biology. Thorp and Covich's Freshwater Invertebrates*, 4 ed.; Thorp, D.; Rogers, D. C., Eds. Academic Press: **2015**; pp 383-421.
2. Gupta, S. K.; Singh, J., Evaluation of mollusc as sensitive indicator of heavy metal pollution in aquatic system: a review. *Environmental Management for Suitainable Development.* **2011,** *2*, 49-57.
3. Krupnova, T. G.; Mashkova, I. V.; Kostryukova, A. M.; Schelkanova, E. E.; Gavrilkina, S. V., Gastropods as potential biomonitors of contamination caused by heavy metals in South Ural lakes, Russia. *Ecological Indicators.* **2018,** *95*, 1001-1007.
4. Schöne, B. R.; Krause, R. A., Retrospective environmental biomonitoring – Mussel Watch expanded. *Global and Planetary Change.* **2016,** *144*, 228-251.
5. Gundacker, C., Comparison of heavy metal bioaccumulation in freshwater molluscs of urban river habitats in Vienna. *Environmental Pollution.* **2000,** *120*, 497-507.
6. Zver'kova, Y. S., Use of freshwater mollusk shells for monitoring heavy metal pollution of the Dnieper ecosystem on the territory of Smolensk oblast. *Russian Journal of Ecology.* **2009,** *40*, 443-447.
7. Gillikin, D. P.; Dehairs, F.; Baeyens, W.; Navez, J.; Lorrain, A.; Andre, L., Inter- and intra-annual variations of Pb/Ca ratios in clam shells (*Mercenaria mercenaria*): a record of anthropogenic lead pollution? *Marine Pollution Bulletin.* **2005,** *50*, 1530-40.
8. Walsh, K.; Dunstan, R. H.; Murdoch, R. N., Differential bioaccumulation of heavy metals and organopollutants in the soft tissue and shell of the Marine Gastropod, *Austrocochlea constricta*. *Environmental Contamination and Toxicology.* **1995,** *28*, 35-39.
9. Cariou, E.; Guivel, C.; La, C.; Lenta, L.; Elliot, M., Lead accumulation in oyster shells, a potential tool for environmental monitoring. *Marine Pollution Bulletin.* **2017,** *125*, 19-29.
10. Puente, X.; Villares, R.; Carral, E.; Carballeira, A., Nacreous shell of *Mytilus galloprovincialis* as a biomonitor of heavy metal pollution in Galiza (NW Spain). *Science of Total Environment.* **1996,** *183*, 205-211.
11. Zuykov, M.; Pelletier, E.; Harper, D. A., Bivalve mollusks in metal pollution studies: from bioaccumulation to biomonitoring. *Chemosphere.* **2013,** *93*, 201-208.
12. Poulain, C.; Gillikin, D. P.; Thébault, J.; Munaron, J. M.; Bohn, M.; Robert, R.; Paulet, Y. M.; Lorrain, A., An evaluation of Mg/Ca, Sr/Ca, and Ba/Ca ratios as environmental proxies in aragonite bivalve shells. *Chemical Geology.* **2015,** *396*, 42-50.
13. Li, D.; Pi, J.; Zhang, T.; Tan, X.; Fraser, D. J., Evaluating a 5-year metal contamination remediation and the biomonitoring potential of a freshwater gastropod along the Xiangjiang River, China. *Environmental Science and Pollution Research International.* **2018,** *25*, 21127-21137.
14. Markich, S. J.; Jeffree, R.; Burke, P., Freshwater bivalve shells as archival indicators of metal pollution fron a copper-uranium mine in tropical northern Australia. *Environmental Science & Technology.* **2002,** *36*, 821-831.
15. Checa, A. G., Physical and biological determinants of the fabrication of molluscan shell microstructures. *Frontiers in Marine Science.* **2018,** *5*, 1-21.
16. Marin, F.; Le Roy, N.; Marie, B., The formation and mineralization of mollusk shell. *Frontiers in Bioscience.* **2012,** *S4*, 1099-1125

17. Zhao, L.; Schöne, B. R.; Mertz-Kraus, R., Controls on strontium and barium incorporation into freshwater bivalve shells (*Corbicula fluminea*). *Palaeogeography, Palaeoclimatology, Palaeoecology.* **2017,** *465*, 386-394.
18. Elliot, M.; Welsh, K.; Chilcott, C.; McCulloch, M.; Chappell, J.; Ayling, B., Profiles of trace elements and stable isotopes derived from giant long-lived *Tridacna gigas* bivalves: Potential applications in paleoclimate studies. *Palaeogeography, Palaeoclimatology, Palaeoecology.* **2009,** *280*, 132-142.
19. Vander Putten, E.; Dehairs, F.; Keppens, E.; Baeyens, W., High resolution distribution of trace elements in the calcite shell layer of modern *Mytilus edulis*: Environmental and biological controls. *Geochimica and Cosmochima.* **2000,** *64*, 997–1011.
20. Thébault, J.; Chauvaud, L.; L'Helguen, S.; Clavier, J.; Barats, A.; Jacquet, S.; Pécheyran, C.; Amouroux, D., Barium and molybdenum records in bivalve shells: Geochemical proxies for phytoplankton dynamics in coastal environments? *Limnology and Oceanography.* **2009,** *54*, 1002-1014.
21. Tabouret, H.; Pomerleau, S.; Jolivet, A.; Pecheyran, C.; Riso, R.; Thebault, J.; Chauvaud, L.; Amouroux, D., Specific pathways for the incorporation of dissolved barium and molybdenum into the bivalve shell: an isotopic tracer approach in the juvenile Great Scallop (*Pecten maximus*). *Marine Environmental Research.* **2012,** *78*, 15-25.
22. Pécheyran, C.; Cany, S.; Chabassier, P.; Mottay, E.; Donard, O. F. X., High repetition rate and low energy femtosecond laser ablation coupled to ICPMS detection: a new analytical approach for trace element determination in solid samples. *Journal of Physics: Conference Series.* **2007,** *59*, 112-117.
23. Russo, R. E.; Mao, X.; Liu, H.; Gonzalez, J.; S. Mao, S., Laser ablation in analytical chemistry - a review. *Talanta.* **2002,** *57*, 425–451.
24. Warter, V.; Muller, W.; Wesselingh, F. P.; Todd, J. A.; Renema, W., Late miocene seasonal to subdecadal climate variability in the Indo-west Pacific (east Kalimantan, Indonesia) preserved in giant clams. *Palaios.* **2015,** *30*, 66-82.
25. Barats, A.; Amouroux, D.; Pecheyran, C.; Chauvaud, L.; Donard, O. F. X., High-frequency archives of manganese inputs to coastal waters (Bay of Seine, France) resolved by the LA-ICP-MS analysis of calcitic growth layers along scallop shells (*Pecten maximus*). *Environmental Science & Technology.* **2008,** *42*, 86–92.
26. Barats, A.; Pecheyran, C.; Amouroux, D.; Dubascoux, S.; Chauvaud, L.; Donard, O. F., Matrix-matched quantitative analysis of trace-elements in calcium carbonate shells by laser-ablation ICP-MS: application to the determination of daily scale profiles in scallop shell (*Pecten maximus*). *Analytical and Bioanalytical Chemistry.* **2007,** *387*, 1131-40.
27. Sturrock, A. M.; Trueman, C. N.; Darnaude, A. M.; E., H., Can otolith elemental chemistry retrospectively track migrations in fully marine fishes? *Journal of Fish Biology.* **2012,** *81*, 766-795.
28. Walther, B.; Limburg, K., The use of otolith chemistry to characterize diadromous migrations. *Journal of Fish Biology* **2012,** *81*, 796-825.
29. Fallon, S.; McCulloch, M.; Van Woesik, R.; Sinclair, D., Corals at their latitudinal limits: laser ablation trace element systematics in Porites from Shirigai Bay, Japan. *Earth and Planetary Science Letters.* **1999,** *172*, 221-238.
30. Hathorne, E. C.; Felis , T.; James, R.; Thomas, A., Laser ablation ICP-MS screening of corals for diagenetically affected areas applied to Tahiti corals from the last deglaciation. *Geochimica et Cosmochimica Acta.* **2011,** *75*, 1490-1506.

31. Massonnet, P.; Heeren, R. M. A., A concise tutorial review of TOF-SIMS based molecular and cellular imaging. *Journal of Analytical Atomic Spectrometry.* **2019,** *34*, 2217-2228.
32. Aoyagi, S., Review of TOF-SIMS bioanalysis using mutual information. *Surface and Interface Analysis.* **2009,** *41*, 136-142.
33. Addadi, L.; Joester, D.; Nudelman, F.; Weiner, S., Mollusk shell formation: a source of new concepts for understanding biomineralization processes. *Chemistry.* **2006,** *12*, 980-7.
34. Gao, P.; Liao, Z.; Wang, X. X.; Bao, L. F.; Fan, M. H.; Li, X. M.; Wu, C. W.; Xia, S. W., Layer-by-layer proteomic analysis of *Mytilus galloprovincialis* shell. *PLoS One.* **2015,** *10*, 1-19.
35. Wilmot, N. V.; Barber, D. J.; Taylor, J. D.; Graham, A. L., Electron microscopy of molluscan crossed-lamellar microstructure *Philosophical Transactions of the Royal Society of London.* **1992,** *337*, 21-35.
36. Kobayashi, I.; Samata, T., Bivalve shell structure and organic matrix. *Materials Science and Engineering.* **2006,** *26*, 692-698.
37. Wang, X.; Li, C.; Zhou, L., Metal concentrations in the mussel *Bathymodiolus platifrons* from a cold seep in the South China Sea. *Deep Sea Research Part I: Oceanographic Research Papers.* **2017,** *129*, 80-88.
38. Pourang, N.; Richardson, C. A.; Chenery, S. R.; Nasrollahzedeh, H., Assessment of trace elements in the shell layers and soft tissues of the pearl oyster *Pinctada radiata* using multivariate analyses: a potential proxy for temporal and spatial variations of trace elements. *Environmental Monitoring Assessment.* **2014,** *186*, 2465-85.
39. Siegele, R.; Orlic, I.; Cohen, D.; Markich, S.; Jeffree, R., Manganese profiles in freshwater mussel shells. *Nuclear Instruments and Methods in Physics Reearch.* **2001,** *181*, 593–597.
40. Markich, S. J.; Jeffree, R. A., Absorption of divalent trace metals as analogues of calcium by Australian freshwater bivalves: an explanation of how water hardness reduces metal toxicity. *Aquatic Toxicology.* **1994,** *29*, 257–290.
41. Bellotto, V. R.; Miekeley, N., Trace metals in mussel shells and corresponding soft tissue samples: a validation experiment for the use of *Perna perna* shells in pollution monitoring. *Analytical and Bioanalytical Chemistry.* **2007,** *389*, 769-76.
42. Takesue, R. K.; Bacon, C. R.; Thompson, J. K., Influences of organic matter and calcification rate on trace elements in aragonitic estuarine bivalve shells. *Geochimica et Cosmochimica Acta.* **2008,** *72*, 5431-5445.
43. Sturesson, U., Lead Enrichment in Shells of *Mytulus Edulis*. *Royal Swedish Academy of Sciences.* **1976,** *5*, 253-256.
44. Ryan, D.; Shephard, S.; Gargan, P.; Roche, W., Estimating sea trout (*Salmo trutta L.*) growth from scale chemistry profiles: an objective approach using LA-ICPMS. *Fisheries Research.* **2019,** *211*, 69-80.
45. Zuykov, M.; Pelletier, E.; Saint-Louis, R.; Checa, A.; Demers, S., Biosorption of thorium on the external shell surface of bivalve mollusks: the role of shell surface microtopography. *Chemosphere.* **2012,** *86*, 680-3.
46. Rainbow, P. S., Trace metal concentrations in aquatic invertebrates: why and so what? *Environmental Pollution.* **2002,** *120*, 497-507.
47. Pan, K.; Wang, W. X., Trace metal contamination in estuarine and coastal environments in China. *Science of the Total Environment* **2012,** *421-422*, 3-16.

List of legends

Figure 1. (a): SEM image of a shell fragment of *Radix balthica* with the outer surface (OS), the inner part (IP) and the inner surface (IS) of the shell in the SEM support (S). (b): SEM image focalised on the OS of the section presented in the image a showing the periostracum with a non-distinct structure of the crystals. (c): SEM image focalised in the IP of the section presented in the image a showing a complex prismatic layer characterised by a crossed lamellar structure of crystals. (d): SEM image focalised in the IS of the section presented in the image a showing a nacreous layer characterised by tablets structure.

Figure 2. Imaging of metal distribution in three biological replicates (R1, R2 and R3) *of Radix balthica* shell cross-section analysed by Fs-LA-ICP-MS. The upper part of the shell represents the outer surface and the bottom part the inner surface of the shell.

Figure 3. Average concentrations ($\mu g \cdot g^{-1}$) of metals (represented by the letter a to g) in the different studied shell layers (Outer Surface - OS, Inner part-IP and Inner Surface – IS, respectively) in the three replicates (R1, R2 and R3) and the average concentrations for the three replicates (Ravg) of *Radix balthica* shell cross-section analysed by Fs-LA-ICP-MS. Significant differences among replicates for each surface are represented by letters a, b and c. Significant Ravg differences are represented by letters A, B and C.

Figure 4. ToF-SIMS mass spectra in positive (a and c) and negative polarity (b and d) of the outer (a and b) and inner (c and d) surfaces of replicate 1 gastropod shell plotted over 0-130 m/z range.

Figure 5. ToF-SIMS depth-profiles (a) of Ca^+ and Ba^+ (x100) metals and organic fragment $C_2H_3^+$ (x10) detected in positive polarity on the outer shell surface of the gastropod *Radix balthica*. The intensity is normalised to the total detected ions count. 3D spatial distribution (b) of Ca^+, Ba^+, and $C_2H_3^+$ reconstructed from the depth-profiles over the analysed area (50 µm x 50 µm = x and y dimensions) versus the etching time (the z axis, 1600 s, which is over dimensioned compared to the other axes).

Graphical abstract:

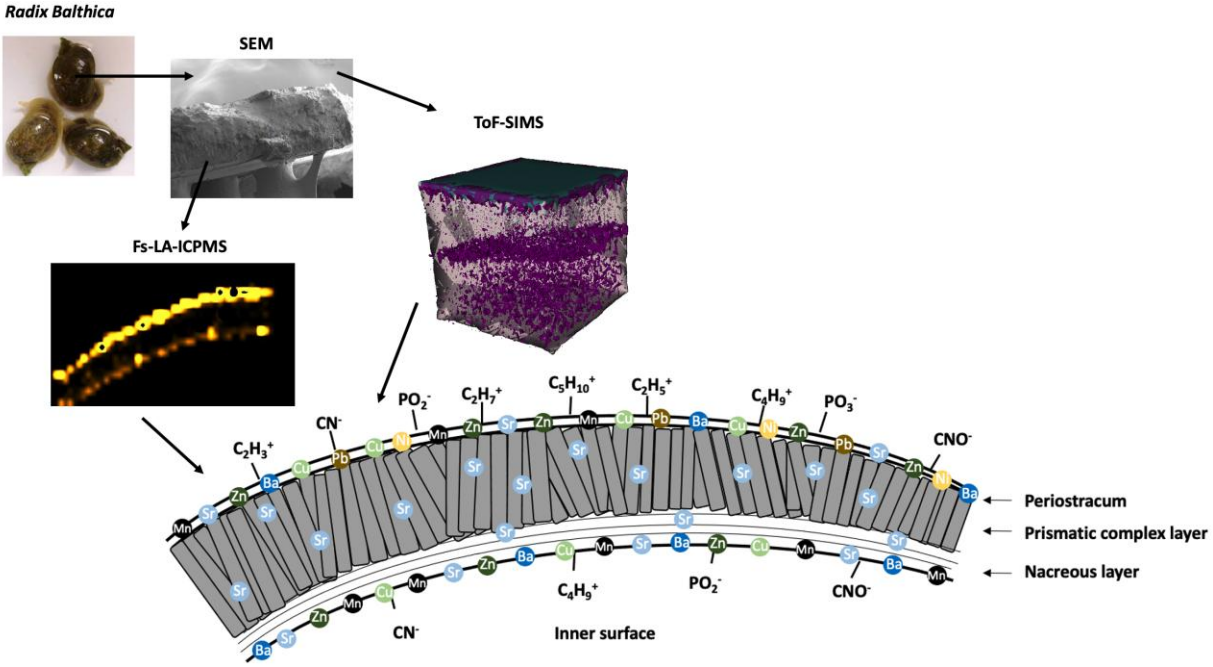

Figure 1:

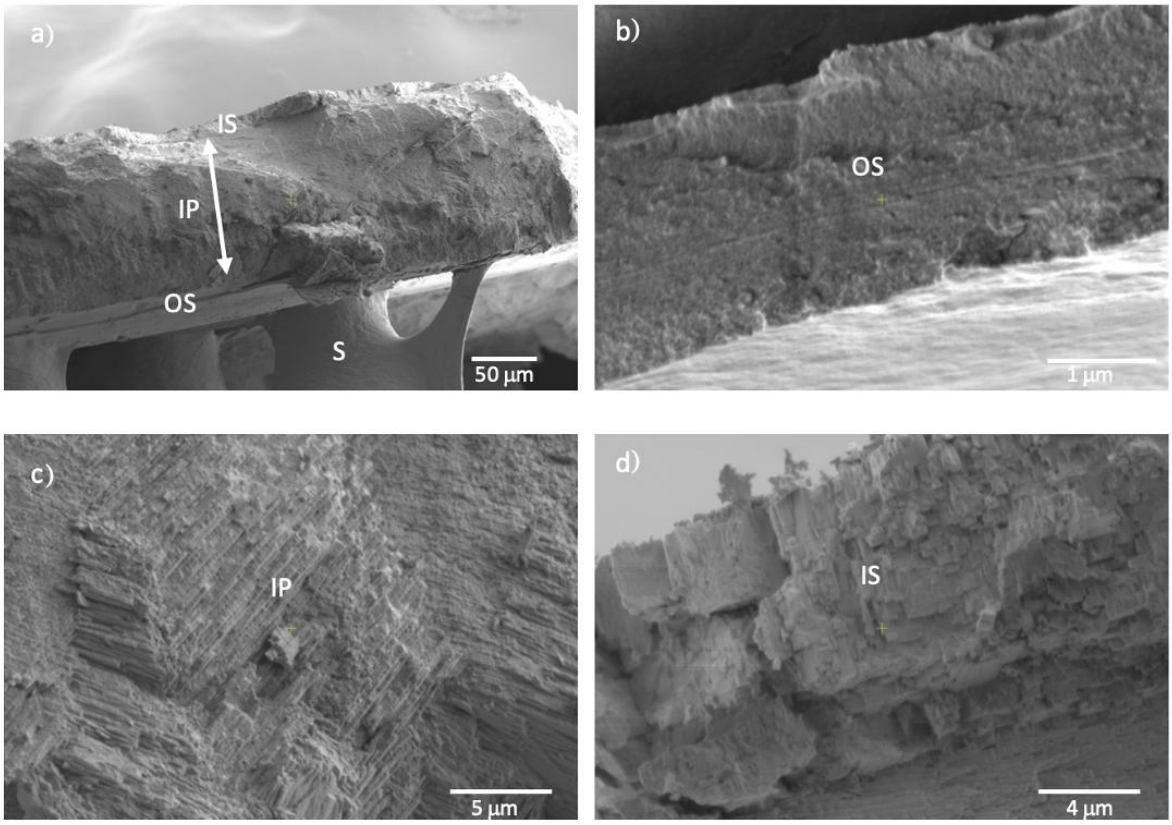

Figure 2:

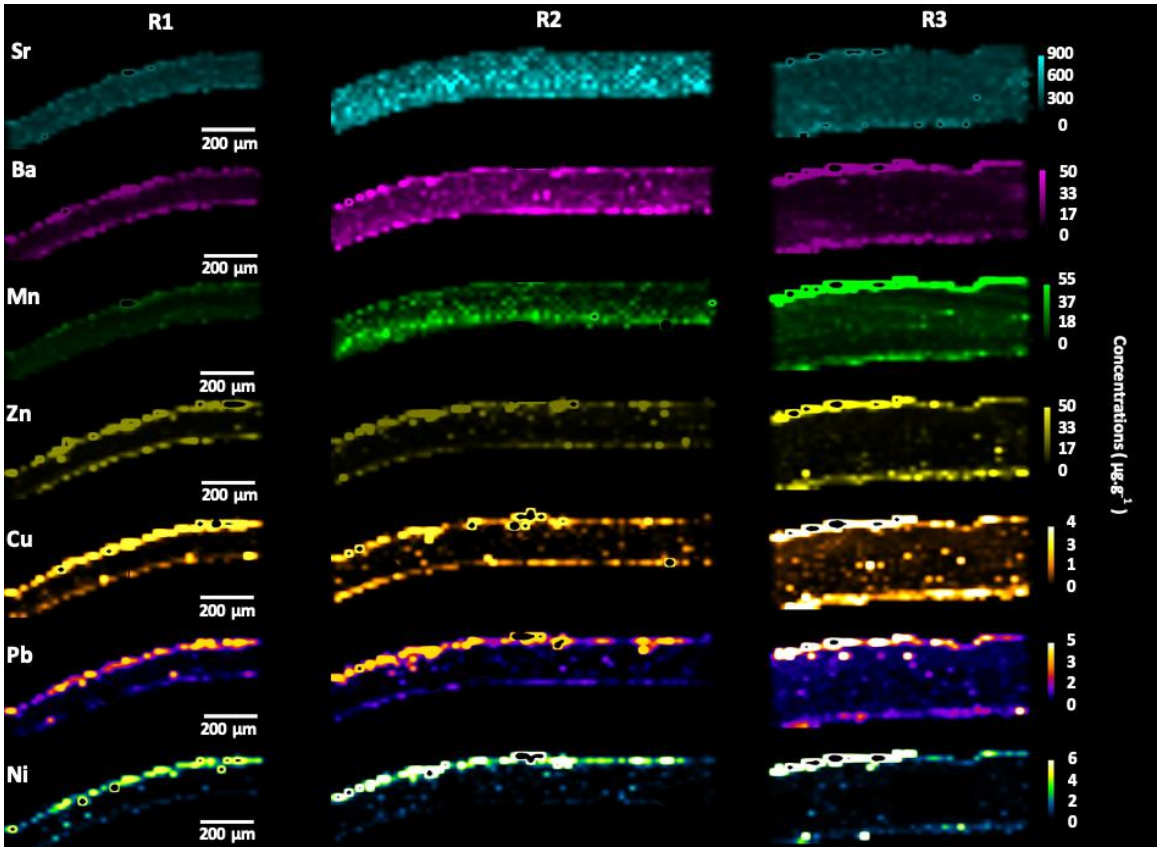
R1
R2
R3
Sr
Ba
Mn
Zn
Cu
Pb
Ni
200 µm
900
600
300
0
50
33
17
0
55
37
18
0
50
33
17
0
4
3
1
0
5
3
2
0
6
4
2
0
Concentrations (µg.g-1)

Figure 3:

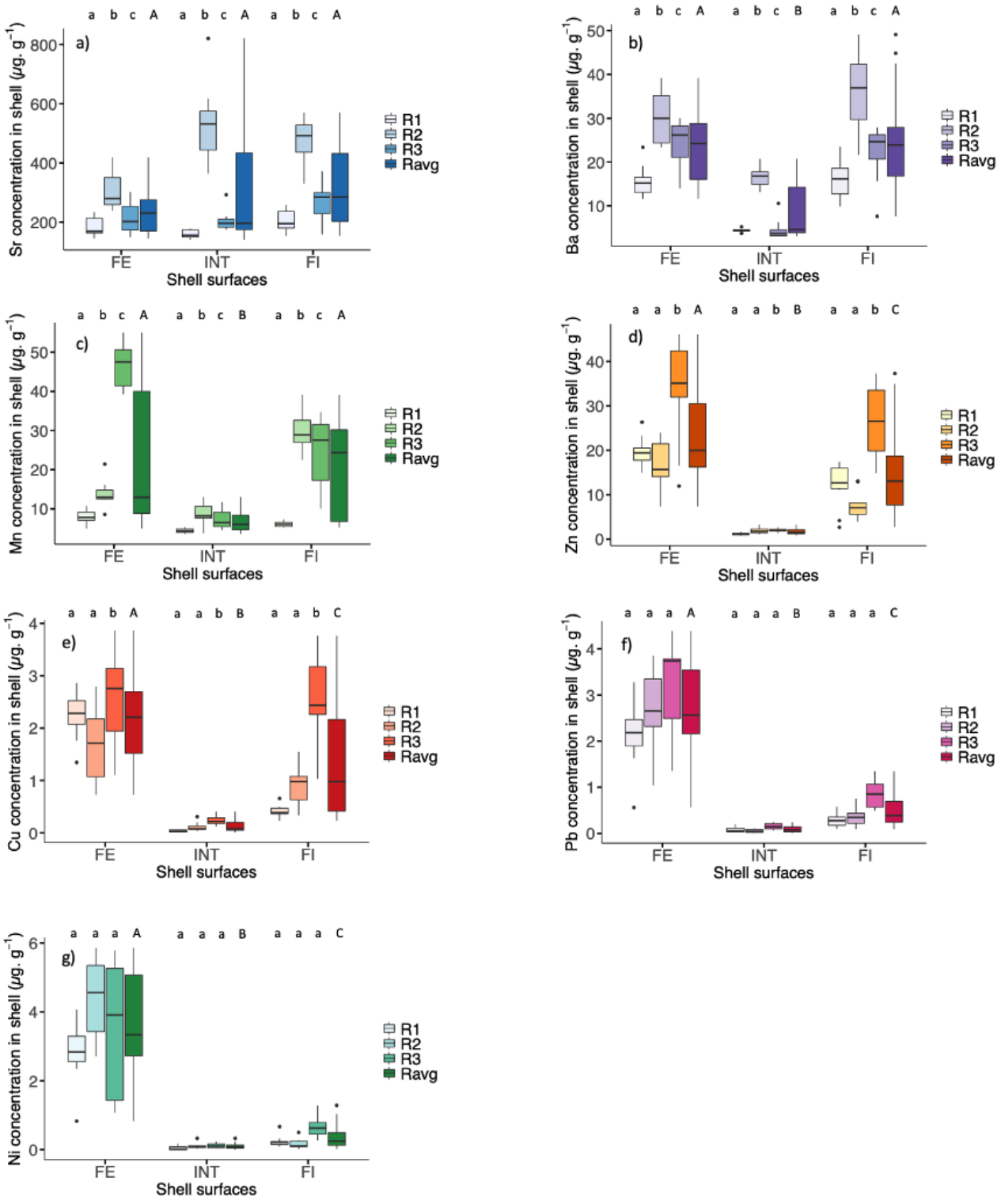
a)
Sr concentration in shell (µg. g⁻¹)
b)
Ba concentration in shell (µg. g⁻¹)
c)
Mn concentration in shell (µg. g⁻¹)
d)
Zn concentration in shell (µg. g⁻¹)
e)
Cu concentration in shell (µg. g⁻¹)
f)
Pb concentration in shell (µg. g⁻¹)
g)
Ni concentration in shell (µg. g⁻¹)
FE
INT
FI
Shell surfaces
R1
R2
R3
Ravg

Figure 4:

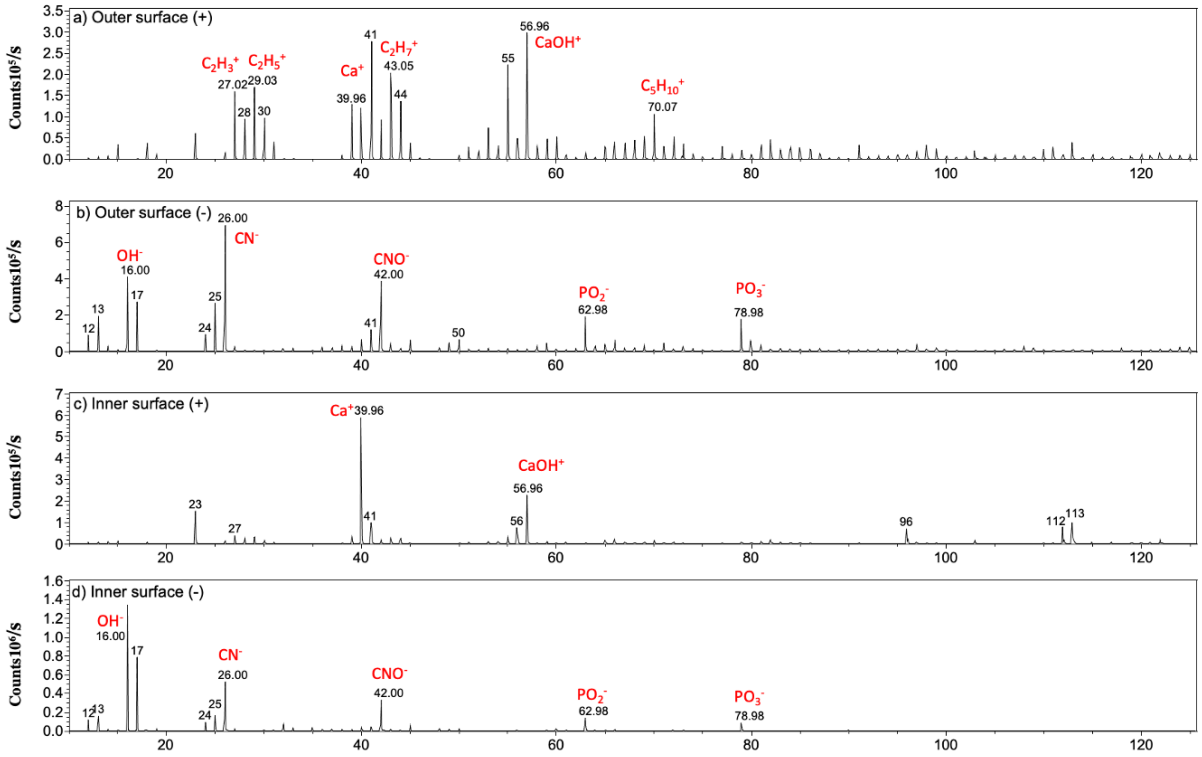

Figure 4: